Characterising natural variability in complex hydrological systems using Passive Microwave based Climate Data Records: a case study for the Okavango Delta

Robin van der Schalie[1], Mendy van der Vliet[1], Clément Albergel[2], Wouter Dorigo[3], Piotr Wolski[4] and Richard de Jeu[1]*

[1]Planet, Haarlem, the Netherlands
[2]European Space Agency Climate Office, ECSAT, Harwell Campus, Didcot, Oxfordshire, UK
[3]CLIMERS, TU Wien, Department of Geodesy and Geoinformation, Vienna, Austria
[4]Climate System Analysis Group, University of Cape Town, Cape Town, South Africa

*** Correspondence:** Robin van der Schalie, rvanderschalie@planet.com

Keywords: Okavango Delta, Passive Microwave Observations, Climate Data Records, Interannual Variability, Surface Soil Moisture, Land Surface Temperature, Vegetation Optical Depth, Land Parameter Retrieval Model

Abstract

The Okavango river system in southern Africa is known for its strong interannual variability of hydrological conditions. Here we present how this is exposed in surface soil moisture, land surface temperature, and vegetation optical depth as derived from the Land Parameter Retrieval Model using an inter-calibrated, long term, multi-sensor passive microwave satellite data record (1998-2020). We also investigate how these interannual variations relate to state-of-the-art climate reanalysis data from ERA5-Land. We analysed both the upstream river catchment and the Okavango Delta, supported by independent data records of discharge measurements, precipitation and vegetation dynamics observed by optical satellites. The seasonal vegetation optical depth anomalies have a strong correspondence with MODIS Leaf Area Index (correlation catchment: 0.74, Delta: 0.88). Land surface temperature anomalies derived from passive microwave observations match best with those of ERA5-Land (catchment: 0.88, Delta: 0.81), as compared to MODIS nighttime LST (catchment: 0.70, Delta: 0.65). Although surface soil moisture anomalies from passive microwave observations and ERA5-Land correlate reasonably well (catchment: 0.72, Delta: 0.69), an in-depth evaluation over the Delta uncovered situations where passive microwave satellites record strong fluctuations, while ERA5-Land does not. This is further analysed using information on inundated area, river discharge and precipitation. The passive microwave soil moisture signal demonstrates a response to both the inundated area and precipitation. ERA5-Land however, which by default does not account for any lateral influx from rivers, only shows a response to the precipitation information that is used as forcing. This also causes the reanalysis model to miss record low land surface temperature values as it underestimates the latent heat flux in certain years. These findings demonstrate the complexity of this hydrological system and suggest that future land surface model generations should also include lateral land surface exchange. Also, our study highlights the importance of maintaining and improving climate data records of soil moisture, vegetation and land surface temperature from passive microwave observations and other observation systems.

1 Introduction

Long-term data records of key components of the climate system, known as essential climate variables (ECV), are important for improving our understanding and predictability of climate behaviour at different time scales (Hollmann et al., 2013; Bojinski et al., 2014). These records can help us to determine the root causes of observed climate change, e.g. natural or anthropogenic, assess its impacts and associated risks, and support mitigation and adaptation activities. In 2008, the European Space Agency (ESA) started the Climate Change Initiative programme (CCI) to develop these ECVs from satellite data records. This was done in response to the United Nations Framework Convention on Climate Change (UNFCCC) need for systematic monitoring of the climate system. Today, the CCI programme covers 21 satellite-based ECV records (Projects (esa.int), last visited September 2021).

Surface soil moisture (SSM) is one of these ESA CCI ECVs. These records are based on a fusion of both passive (PMW) and active microwave satellite retrievals (Dorigo et al., 2017). The current version 6.1 spans from 1979 until 2020 (Scanlon et al., 2021), and contains three separate SSM products, which are derived from active, passive, and a combination of active and passive sensors. The methodology and evaluation of the harmonisation and merging of the soil moisture retrievals from multiple satellites is described by Gruber et al. (2019). ESA CCI SSM data has been used for more than 10 years as the baseline for the annual evaluation and interpretation of global SSM conditions as reported in the leading "State of the Climate" reports (Van der Schalie et al., 2021) that are published as a supplement to the Bulletin of the American Meteorological Society. Three datasets are produced as part of the passive input for the ESA CCI SM, which is SSM (SSM_{MW}), but also land surface temperature (LST_{MW}), and vegetation optical depth (VOD_{MW}).

SSM_{MW} data sets have been extensively evaluated with ground observations, models, other satellite products, and related ECVs like precipitation (e.g. Hirschi et al., 2021; Beck et al., 2021; Dorigo et al., 2015; Al-Yaari et al., 2019; Albergel et al., 2013; Loew et al., 2013). VOD_{MW} has been used in multiple studies with a focus on seasonal and interannual vegetation dynamics (e.g. Liu et al., 2015; Moesinger et al., 2020; Teubner et al., 2019) or specifically on L-band VOD characteristics (e.g. Schwank et al., 2021; Bousquet et al., 2021; Rodriguez-Fernandez et al., 2018). Research on the quality of LST_{MW} (e.g. Holmes et al., 2009; Holmes et al., 2015) remains limited. The robustness of the interannual variability signals within these multi-decadal data records is still not always clear, and a combined assessment of all three variables is necessary for understanding these datasets, as the current joint retrieval algorithm make their values fundamentally intertwined (Owe et al., 2008). Such information provides unique opportunities for both monitoring and seasonal forecasting, e.g. over Africa (e.g. Cook et al., 2021).

The purpose of this paper is to improve insight into the interannual signals of the SSM_{MW}, LST_{MW} and VOD_{MW} by presenting a case study over a region with a complex hydrological system, i.e. the Okavango, and how their skill compares to state-of-the-art climate reanalysis data from ERA5-Land (Muñoz-Sabater, 2019; Muñoz-Sabater, 2021). ERA5-Land aims to quantify the water and energy cycles over land in a consistent manner, therefore allowing the characterisation of trends and anomalies. Although ERA5-Land (E5) data is known to be of high quality in many regions around the globe, for use in any specific regions this needs to be properly evaluated. Therefore, this dataset does not only function as a benchmark in this study, but will also be analysed in more detail to evaluate its ability to properly detect the natural dynamics and variability in the Okavango and how this compares to the signal of the passive microwave-based datasets. Other datasets are used as support for determining which dataset (i.e., either PMW or E5L estimates of the same variable) is more likely to reflect true conditions. This research can help to improve the synergy between EO data sets and land surface models, and to identify both strengths and shortcomings of either one.

More specifically, the Okavango Delta and Okavango River Catchment in southern Africa were selected as the study area. The Okavango Delta (Republic of Botswana, 2013) consists of permanent marshlands and seasonally flooded plains, and is one of the few endorheic "delta" systems (geomorphologically Okavango Delta is an alluvial fan, Kgathi et al. 2006) that does not flow into the ocean. It is an exceptional example of the interaction between climatic, hydrological and biological processes, leading to a unique mix of flora and fauna, and has therefore been included in the UNESCO World Heritage List since 2014. Three features in the local hydrological system stand out, i.e., the strong interannual variability, the lateral water influx component of the Okavango River into the Delta, and the seasonal characteristics with a lag between rainfall, river discharge and flooding. Unfortunately, it is expected that global warming will affect this natural variability in the hydrological cycle over the Okavango Delta (Wolski et al., 2014; Wolski et al., 2012), for example reducing high-water periods like in 2009-2011. These kinds of negative impacts increase the need for reliable monitoring capabilities.

The structure of the paper is as follows. Section 2 introduces the study area and includes the exact regions of interest (ROIs) that are used for the data extraction. Sect. 3.1 describes the passive microwave data and other data sources. Sect. 3.2 explains the methodology, concerning the inter-calibration (3.2.1), the Land Parameter Retrieval Model (LPRM, 3.2.2), evaluation of the dataset anomalies (3.2.3.), and of the river, flood and precipitation contribution to SSM anomalies over the Okavango Delta (3.2.4). Sect. 4, 5 and 6 provide the Results, Discussion and Conclusions of these different steps.

2 Research Area

With a length of approximately 1600 km, the Okavango river is one of the largest in southern Africa (Muzungaire et al. 2012). The river is known globally for its large terminating inland "delta". The Okavango Delta is a large seasonally pulsed inland wetland, a mixture of aquatic vegetation, open water, and dry land with the actively inundated area covering a part of the 28,000 km^2 alluvial cone (Ringrose et al., 1988).

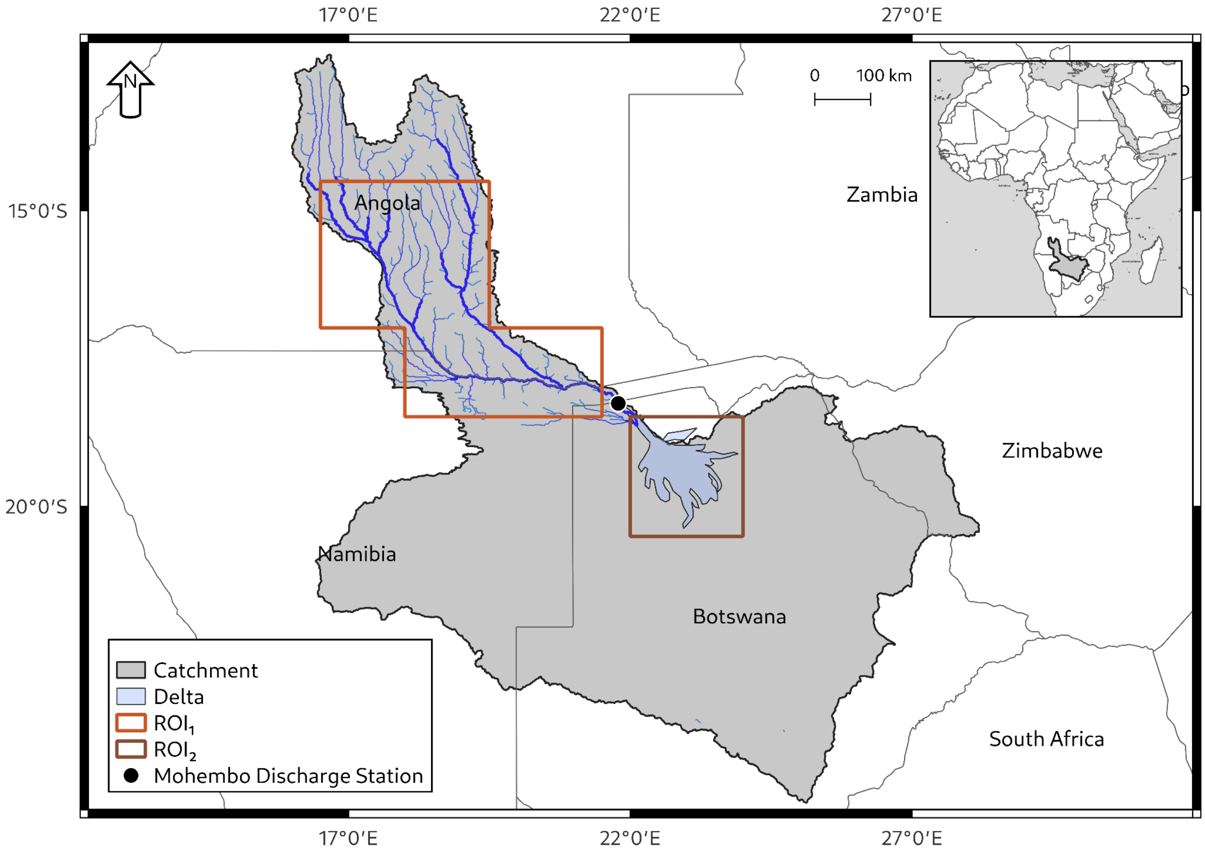

Figure 1: The research area comprising ROI_1 (a part of the upstream area of the Cubango and the Cuito River) and ROI_2 (the surrounding of the Okavango Delta) in relation to the Okavango drainage basin (grey). The black dot marks the location of the discharge station at Mohembo.

In line with both the interannual variation in local and upstream rainfall and the longer-term effects of surface-groundwater interactions, substantial interannual variability in the Delta's inundated area was recorded over the period 1932-2000 (Wolski and Murray-Hudson, 2008), with annual minima of about 3000 km^2 up to annual maxima of 12000 km^2 (Wolski et al., 2017; Gumbricht et al., 2004). Whereas estimates for the total annual water budget stemming from direct rainfall in the Okavango Delta ranges between 25% to 50%, the Okavango River inflow accounts for the other 50% to 75% (McCarthy et al., 1998; McCarthy et al., 2000; Ashton and Manley, 1999; Ashton and Neal, 2003, Wolski et al., 2006).

In this study we focus on only two perennial rivers in the Okavango catchment - the Cubango River and the Cuito River (Ashton and Neal, 2003). Data was extracted from the catchment area within ROI_1 of Figure 1. These rivers originate in Angola and are a vital lifeline to the Okavango Delta with an average yearly inflow at Mohembo of 9863 millions of m^3 (approximately 300 m^3/s) in the period 1932-2001 and a 71.4% contribution to the total water budget of the Delta.

The Angolan part of the basin is characterised by a subtropical climate, while in Botswana and Namibia parts are classified as semi-arid (Kgathi et al. 2006). During drought years in the 1980s and 1990s, the annual inflow at Mohembo reduced up to 45% (McCarthy et al., 2000;

Ashworth, 2002; Ashton, 2003; Ashton and Neal 2003) which then coincided with proportional declines of the Okavango Delta outflow to the Thamalakane and Boteti rivers (Ashton & Manley 1999; Ashworth 2002, Ashton and Neal 2003). Throughout these periods a growing demand for water arose in Botswana and Namibia (MGDP, 1997; Ashton, 2003). Overall, the dry phase was caused by multi-decadal oscillations in rainfall, and likely related to processes of internal variability in the climate system (Wolski et al., 2012).

ROI_1 and ROI_2 were chosen to study how their significantly different water influxes affect the signal of the data sources used in the evaluation. The Delta is of particular interest, as it is mostly driven by a strong and highly variable lateral influx from the Okavango River that creates a pattern of seasonally varying wetness that is asynchronous or off-phase with the rainy season.

3 Material and Methods

3.1 Data

3.1.1 Passive microwave observations

The three main variables that are used for the analysis are surface soil moisture (SSM_{MW}), vegetation optical depth (VOD_{MW}) and land surface temperature (LST_{MW}). These variables are derived from passive microwave observations from multiple satellite sensors that observe in similar frequencies and overlap in time.

The Advanced Microwave Scanning Radiometer for EOS (AMSR-E, Kawanishi et al., 2003) is a twelve-channel, six-frequency, passive microwave radiometer developed by the Japan Aerospace Exploration Agency (JAXA) and was active between 2002 and 2011. AMSR-E is part of the payload carried onboard the Aqua (EOS PM-1) NASA scientific research satellite, which has a polar orbit with a 1:30 pm / am equatorial crossing time for ascending / descending swaths. AMSR-E was launched to obtain data to improve our understanding of global-scale water and energy cycles and played a key role in the development of soil moisture retrieval algorithms. For the technical specifics, see Table 1. Only descending brightness temperature data was used for this study, as due to the thermal equilibrium during night time, these are more stable and of higher quality (Owe et al., 2008; Van der Schalie et al., 2021).

The Advanced Microwave Scanning Radiometer 2 (AMSR2, Imaoka et al., 2012) onboard the GCOM-W1 satellite is the follow-up of AMSR-E, and was launched in 2012. Although incorporating improvements, both the general setup and orbital characteristics (e.g. overpass times) are similar to AMSR-E (see Table 2). However, unfortunately there is a gap between AMSR-E and AMSR2 of about 9 months, making a direct intercalibration of time series complicated.

To overcome this gap and to extend the passive microwave observation record back to 1998, we make use of the Tropical Rainfall Measuring Mission's (TRMM, Kummerow et al., 1998) Microwave Imager (TMI). TMI observes in X-band and higher frequencies. TRMM is not in a polar orbit because of its focus on the Tropical regions and therefore does not cover the entire globe. Data is only available between 40°N and 40°S and due to its orbital characteristics has a variable crossing time, see Table 1. To find a good balance between data availability and data stability (the more stable temperature distribution between the soil and vegetation close to thermal equilibrium), only brightness temperature data was used that had a local overpass time between 10:30 pm and 4:30 am, to best match AMSR-E and AMSR2.

For this study we use VOD_{MW} and SSM_{MW} derived from X-band brightness temperature data due to its availability on all three sensors, while Ka-band is the main frequency used for the LST_{MW}. All brightness temperatures were collected and gridded into a 0.25° grid for the study area.

Table 1: Overview and characteristics of passive microwave satellite sensors used in the study.

Sensor	Provider	Temporal coverage	Bands	Spatial coverage	Swath Width	Equatorial crossing time	Data level	Footprint size (X, Ka)
Advanced Microwave Scanning Radiometer for EOS (AMSR-E) on AQUA	JAXA / NASA	07/2002 – 10/2011	C, X, Ku, K, Ka, W	Global	1445 km	Asc: 13:30 Desc: 1:30	L2A v3	40 km, 11 km
Advanced Microwave Scanning Radiometer 2 (AMSR2) on GCOM-W1	JAXA / NASA	05/2012 – ongoing	C, X, Ku, K, Ka, W	Global	1450 km	Asc: 13:30 Desc: 1:30	L1R	33 km, 10 km
Tropical Rainfall Measuring Mission's (TRMM) Microwave Imager (TMI)	NASA	01/1998 – 12/2013	X, Ku, K, Ka, W	N40° to S40°	780 km (897 after orbit boost 2001)	Varies (non polar-orbit)	L1C (XCAL, Berg et al., 2016)	50 (58) km, 13 (14) km

3.1.2 Ancillary data sets

In our analysis we use several ancillary data sets to determine the ability of passive microwave-based satellite data records to correctly capture interannual variations. These ancillary datasets are split into two types:

Firstly, data was used from the ERA5-Land climate reanalysis model (Muñoz-Sabater, 2019; Muñoz-Sabater, 2021), which is an enhanced resolution (9 km x 9 km) land-only offline rerun of the ECMWF ERA5 climate reanalysis (Hersbach et al., 2020). SSM_{E5}, LST_{E5} and PR_{E5} were extracted. For both SSM_{E5} and LST_{E5} the Layer 1 (0-7cm) was used. LAI_{E5} was excluded from the analysis as it only contained a climatology based on satellite EOs (no interannual variability). ERA5-Land data was extracted from the Copernicus Climate Change Service (C3S) Climate Data Store (CDS). As it has an hourly resolution, the values closest to the satellite overpasses were chosen. Data covers the complete period of 1998 to 2020.

Secondly, independent observational datasets are used, which have the sole purpose of functioning as a benchmark. These consist of the Okavango River Discharge measurements (ORD, Okavango Research Institute, 2021), Okavango Delta Inundated Area ($ODIA_{MD}$), Leaf

Area Index (LAI_{MD}, Yang et al., 2006) and nighttime LST (LST_{MD}, Wan, 2014) from the Moderate Resolution Imaging Spectroradiometer (MODIS), and precipitation from the NASA Global Precipitation mission's IMERG product (PR_{IM}, Huffman et al., 2015).

A majority of the water entering the Okavango Delta originates from the Delta inlet at Mohembo. Therefore, we use ORD from the Mohembo station (see Fig. 1) to indicate the long term variability of the lateral inflow into the Delta. Measurements, using E-type gauge plates, are done on a regular (fortnightly) basis by the Botswana Department of Water Affairs, and the data are shared by the Okavango Research Institute of the University of Botswana. The advantage of using this data set is that it has a long historical record dating back to 1974. For this study, data was extracted for the 1998 to 2020 period.

$ODIA_{MD}$ represents the inundated area in the Okavango Delta, and is derived from using shortwave infrared (SWIR) observations from the MODIS sensor (Wolski et al., 2017). More specifically data for band b7 from the MCD43A4 product was used. Reflectances of training areas are used to dynamically determine the threshold used for the derivations of the inundation. An automated and up to date monitoring tool for the flooding extent can also be found online (http://www.okavangodata.ub.bw/).

The LAI_{MD} is defined as the one-sided green leaf area per unit ground area (Chen et al., 1992; Yang et al., 2006). The LAI_{MD} for the study area, including both the drainage Catchment and the Delta, was extracted from the MOD15A2H Version 6 MODIS dataset. This is an 8-daily product that uses the best available pixel within the 8-day period. The product has a spatial resolution of 500 m, and the mean was extracted for the complete ROIs.

1 km nighttime, about 1:30 am, surface temperature from MODIS was extracted from the MYD11A2.006 product, which is based on the average over 8 days of all available LST_{MD} observations. For this study the mean values of the two areas were extracted. The temporal coverage is from February 2000 to the end of 2020 for the LAI_{MD} and July 2002 to the end of 2020 for the LST_{MD}.

For PR_{IM}, data was used from the Integrated Multi-satellitE Retrievals for GPM (IMERG, Huffman et al., 2015), which is produced at 0.1° resolution. IMERG is a unified algorithm that provides rainfall estimates based on a combination of observations from multiple passive-microwave sensors, infrared sensors and precipitation gauges. Mean daily data was used from the GPM_3IMERGDF version 6, covering June 2000 to December 2020.

3.2 Methods

3.2.1 Intercalibration of PMW brightness temperatures

The intercalibration of AMSR-E, AMSR2 and TRMM is based on the methodology described in Van der Schalie et al. (2021). In this approach a two-step linear regression model is used, which first defines a global slope and afterwards a local intercept. Secondly, it uses a cost function that not only minimises the differences between brightness temperatures of the individual polarizations, i.e. vertical (V) and horizontal (H), but also for the ratio between the two. This is because the Land Parameter Retrieval Model (LPRM, see next section) used for the SSM_{MW}, VOD_{MW} and LST_{MW} retrievals is very sensitive to the polarisation ratio. Inconsistencies in this ratio between different sensors can lead to an imbalance in how the radiative transfer model distinguishes between the emission from the soil and the from vegetation, respectively, leading to biases in the resulting retrievals. This intercalibration methodology was, previously only applied only to the Ku-, K- and Ka-band, but isis here also used for applied to the X-band data in the same way.

More specifically, the following cost function is minimised in the linear regression instead of a standard least squares approach:

$$Err = \sum_{\square}^{\square} RMSE\,TB_H + \sum_{\square}^{\square} RMSE\,TB_V + 500 * \sum_{\square}^{\square} RMSE\,MPDI \qquad (1)$$

with:

$$RMSE\,TB_{H/V} = \sqrt{\square} \qquad (2)$$

$$RMSE\,MPDI = \sqrt{\square} \qquad (3)$$

Where TB is the brightness temperature for the two polarisations and from the base (s1) and calibrated (s2) satellite. The α and β are the slope and intercept for the linear regression. The T refers to the time steps with overlapping observations for a single location.

After retrieving sensor specific SSM_{MW}, VOD_{MW} and LST_{MW} from the inter-calibrated TB, a linear regression is applied between the different sensors using their respective overlap to remove any leftover inconsistencies. Improved inter-calibration between sensors can lead to a reduced need for break corrections (e.g. Preimesberger et al., 2020) and help to better address related issues at the source.

As this study focuses on anomalies at a seasonal timescale, the temporal coverage obtained by the current three sensors is sufficient. However, as was shown by Van der Schalie et al. (2021) and as is done for the passive microwave based data input for the ESA CCI SM, other sensors like GPM, FengYun-3B and FengYun-3D can be included without issues, resulting in improved revisit times and coverage.

3.2.2 Land Parameter Retrieval Model

The Land Parameter Retrieval Model (LPRM, Owe et al., 2008) is a retrieval algorithm that simultaneously solves for SSM_{MW}, VOD_{MW} and LST_{MW} without the use of any ancillary data sources on vegetation or temperature. The model is based on the tau omega (τ-ω) model (Mo et al., 1982), which simulates the top-of-the-atmosphere brightness temperatures by modelling the individual contribution of the soil, vegetation and atmosphere. LPRM mainly distinguished itself from other algorithms through the analytical derivation of the VOD (Meesters et al., 2005) and the use of Ka-band observations for the LST_{MW} (Holmes et al. 2009). Here we use version 6.0 of LPRM, as developed by Van der Schalie et al. (2017).

LPRM is currently the main algorithm used for all the passive microwave-based SSM retrievals in ESA CCI SM (Dorigo et al., 2017). Due to its unique analytical solution for the derivation of VOD_{MW} that uses no external source of information for the vegetation, LPRM has also been used in several studies of long term vegetation dynamics (Liu et al., 2012; Liu et al., 2015), land degradation (Liu et al., 2013; Van Marle et al., 2017) and the development of climate data records of VOD_{MW} like the VOD Climate Archive (VODCA, Moesinger et al., 2020).

3.2.3 Evaluation of anomalies

To have a better understanding of the quality of the different datasets in detecting interannual variability and anomalies, a two-step comparison analysis is done. First, the anomalies are visualised over time and their dynamics assessed. Second, the relations between related datasets are quantified using correlations and visualised using density plots. This is done separately for the catchment and the delta.

The SSM_{MW} is compared to the SSM_{E5}, both representative for the moisture conditions in the first few centimetres of the soil. As this is a direct comparison, in this step the focus will be on their similarity and differences, without analysing what causes it. Additionally, an extensive analysis is conducted (Section 3.2.4) to determine which of the data sets most likely reflects the ground conditions, based on their relation to ORD, $ODIA_{MD}$ and PR.

For VOD_{MW} there is a comparison with another regularly used satellite-based datasat, LAI_{MD}. Theoretically the VOD_{MW} represents the attenuation of the microwave emission through the vegetation cover, which is related to both the structure and moisture content of the vegetation. The LAI_{MD} is representative of the projected single-sided green leaf area per unit ground area. Although VOD and LAI are fundamentally different, it is assumed that for dynamic and sparsely to moderately vegetated regions, i.e. excluding forests, the X-band also mostly measures the response of the leaves with the microwave signal via the vegetation water content (Jackson & Schmugge, 1991). Further defining the quality and ability of VOD_{MW} to detect interannual variability can be especially useful in improving the applicability and understanding of independent vegetation data records based on passive microwave observations like VODCA (Moesinger et al., 2020).

Here the anomalies of LST from three different sources, e.g. passive microwave (LST_{MW}), model ($LST_{E5,}$) and thermal infrared (LST_{MD}) are evaluated. These represent slightly different parts of the soil surface, being 0 - 7 cm, 0 - 0.1 cm and 0 cm (skin) respectively. The mismatch in depth is also a reason why we choose for night time comparisons, as there is much more thermal stability. When looking over longer periods (e.g. weeks, months) we assume that the slightly different definitions of the soil temperature should still show a similarity in underlying anomalies, as in correlating well.

Because the focus is on the (seasonal) variability over a multi-decadal timespan, a 91 day moving average (±45 days) is first applied to the data sets. The climatology for the anomaly calculation is based on the 2003-2020 period, as the LST_{MD} is only available from 2003 onwards and overall consistency for the baseline is preferred. As the window for the moving average is 91 days, little impact is assumed from data loss due to cloud cover in the MODIS datasets.

It is worth keeping in mind that none of these datasets provide the “truth” or measure exactly the same quantity, therefore differences are to be expected. In the analysis component (see following Section), extra attention will be given to a specific case in the Okavango Delta where a clear divergence is observed between the different SSM datasets.

3.2.4 Analysis of river flooding and precipitation contribution to soil moisture anomalies in the Okavango Delta

As further in this study (Sect 4.1) the signal of the two SSM data sources (SSM_{MW} and SSM_{E5}) is shown to diverge over the Okavango Delta, an in-depth analysis is set up to explain the main drivers of their respective signals. This can help to better understand what the SSM data sets represent and give users insight in how to use them for their research activities and applications.

A first step in this is to directly compare the SSM data sets to the ORD, $ODIA_{MD}$ and both PR_{E5} as PR_{IM}. These data sets can provide insight into what is the driver of the SSM anomalies in this region. As described in section 2, about 50%-75% of the total influx of water into the Okavango Delta comes from the ORD, while PR on average contributes 25%-50%, so we expect to see this reflected in the SSM either via the ORD or the $ODIA_{MD}$ signals.

Following this, a multiple linear regression exercise is conducted. This is done to look into the influence of the $ODIA_{MD}$, ORD and PR signals on the SSM_{MW} and SSM_{E5} anomalies in the Delta. This allows us to determine the drivers of the SSM anomalies, and more importantly, how they differ between the two. Instead of using the absolute anomalies in this analysis, the Z-score is preferred, as this normalisation removes issues with conversion of units and can be interpreted as standardised anomalies. A visualisation will also be made of the climatologies from the different datasets, including their 10 and 90 percentiles, to further define the connection and time lag between the signals of the different parameters.

4 Results

4.1 Soil Moisture

Figure 2 shows the anomalies of SSM_{MW} and SSM_{E5} over the Okavango catchment and Delta, with Figure 2E/F comparing them directly to each other in a density plot. In both areas the two datasets correlate moderately well, 0.72 and 0.70 respectively. In the Delta however, a mismatch occurs on some occasions, leading to a visible flat line in the density plot where the anomalies of SSM_{MW} vary while the anomalies of SSM_{E5} are close to 0 (Fig. 2E). The signal SSM_{MW} anomalies over the Catchment, and SSM_{E5} anomalies over both the catchment and Delta, seem to have clear short-term variability as can be seen from the peaks in the wet season, while the dry season remains mostly stable around 0. Only the anomalies of SSM_{MW} over the Delta diverge from this and show a more multi-year variation, with highs in the years around 2011 and lows in the early and late periods of the time period. These cases will be further analysed in Sect. 4.4 in combination with the ORD and PR.

The absolute range of the anomalies differs to some extent between the two products: SSM_{MW} anomalies range between -0.03 and 0.025 m^3m^{-3} in the Catchment and -0.05 and 0.05 m^3m^{-3} in the Delta, whereas SSM_{E5} anomalies range between -0.10 and 0.06 m^3m^{-3} in the Catchment and -0.08 and 0.10 m^3m^{-3} in the Delta. However, the dynamics of the signal are very similar.

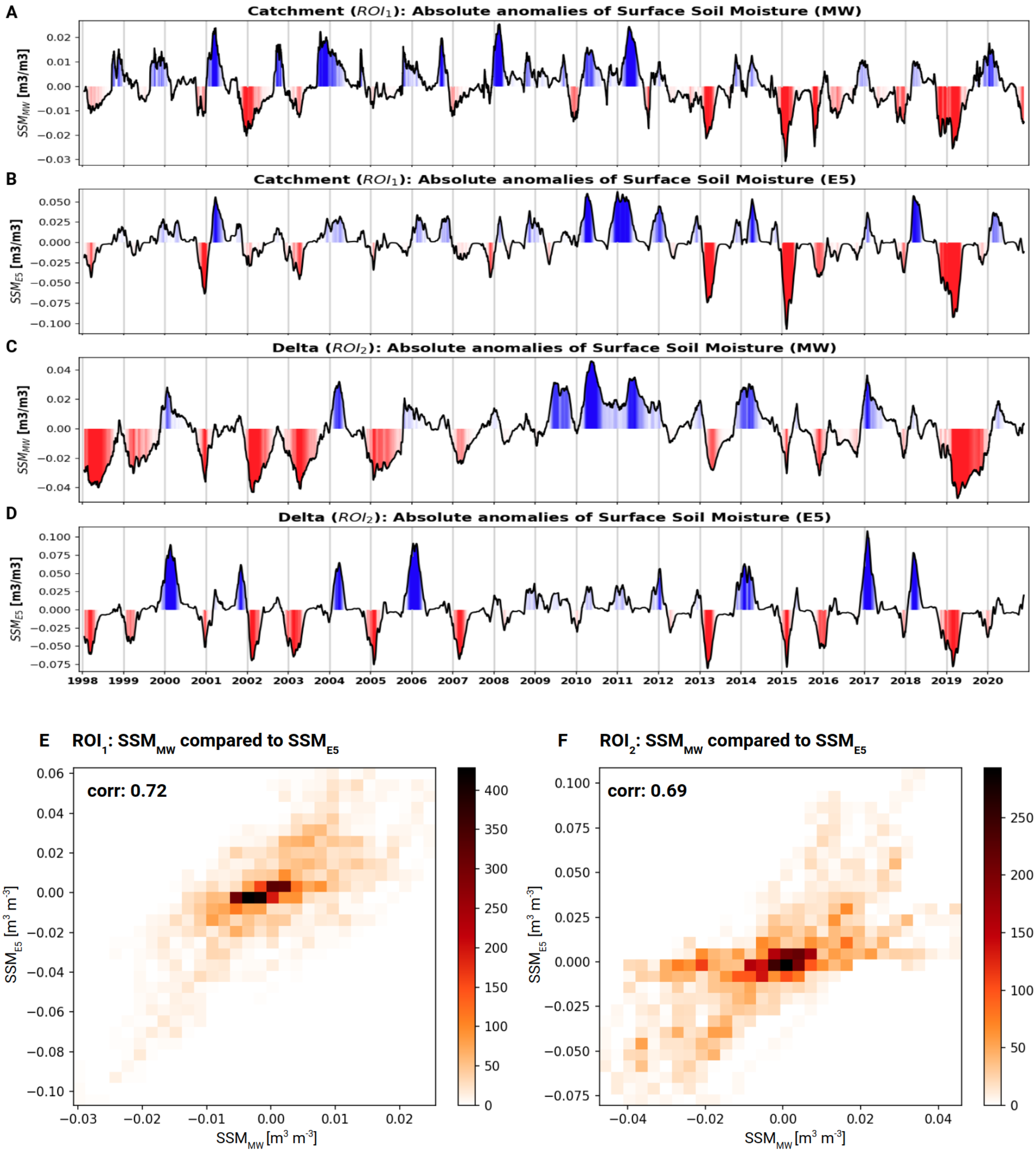

Figure 2: SSM$_{MW}$ and SSM$_{E5}$ absolute anomalies over the Okavango Catchment (A,B,E), with the intensity of the colouring based on the z-score of the positive (blue) and negative (red) anomalies, and the Okavango Delta (C,D,F) in time series and density plots. A daily time step is used from the moving average data set.

4.2 Vegetation Optical Depth

Figure 3 shows the anomalies of VOD$_{MW}$ and LAI$_{MD}$ over the Okavango Catchment and Delta, with Figure 3E/F again showing a direct comparison in a density plot. The two datasets have a 0.74 correlation over the Catchment and up to 0.88 in the Delta. Generally, a similar pattern is visible for both regions. One exception can be seen during the 2008 to 2011 period in the Catchment, where the VOD_{MW} anomaly remains high throughout multiple years, while the overall above average LAI_{MD} anomalies fluctuate to a greater extent. The lowest values in the Delta were detected early in the study period, with VOD_{MW} recording an almost -0.08 anomaly during 1998 and 2003. This 2003 event is also seen in the LAI_{MD} dataset, while no data is available for 1998. In more recent years, no negative anomalies of that strength have been recorded.

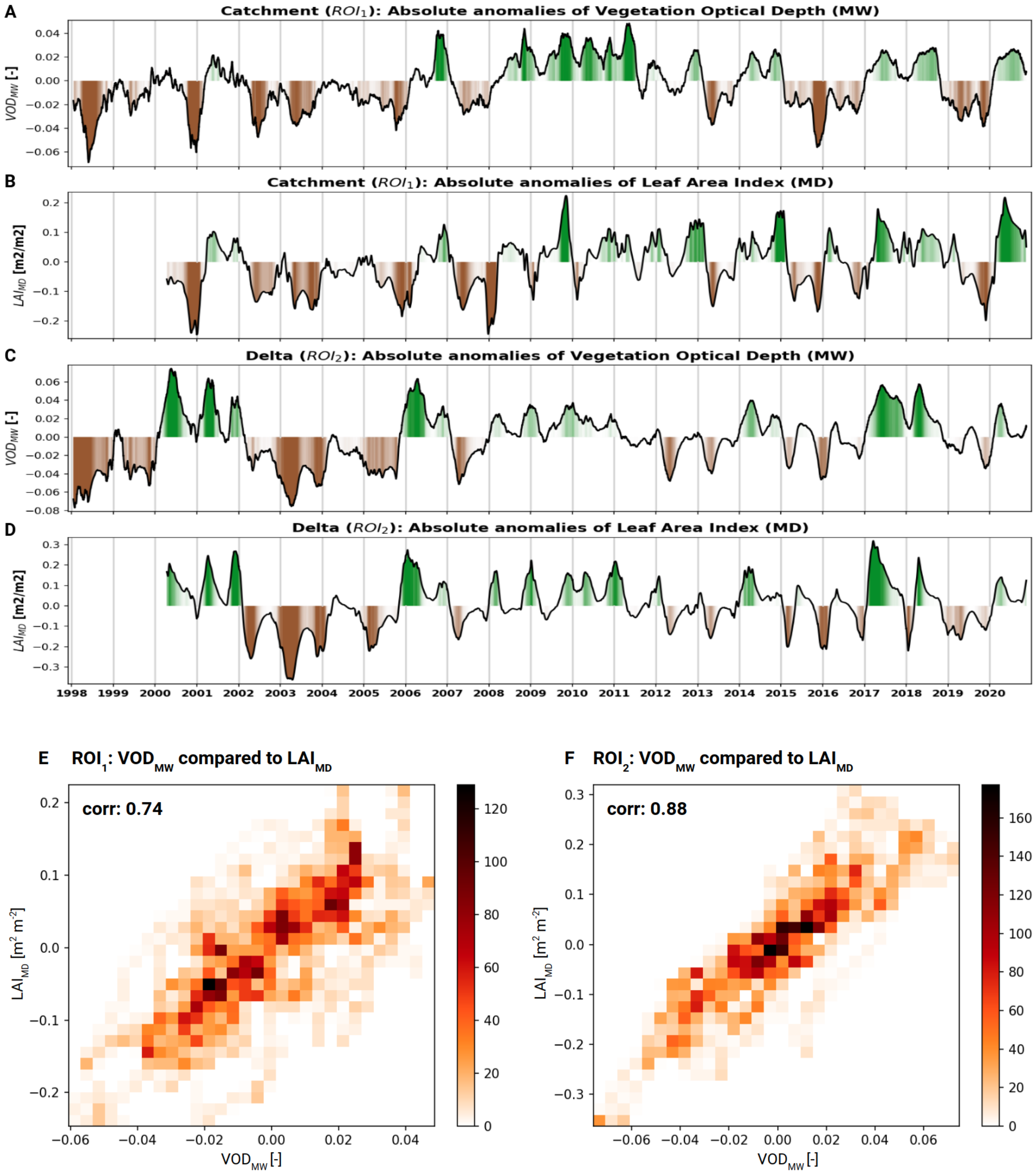

Figure 3: VOD_{MW} and LAI_{MD} anomalies over the Okavango Catchment (A,B,E), with the intensity of the colouring based on the z-score of the positive (green) and negative (brown) anomalies, and the Okavango Delta (C,D,F) in time series and density plots. A daily time step is used from the moving average data set.

4.3 Land Surface Temperature

Figure 4A/B shows the anomalies of LST_{MW} over the Okavango Catchment and Delta, with Figure 4B/C/D/E/F/G showing a direct comparison in a density plot between LST_{MW}, LST_{E5} and LST_{MD}. Because of the high correlation between LST_{MW} and LST_{E5}, of 0.88 in the Catchment and 0.81 in the Delta, the decision was made to only show the LST_{MW} time series to focus more on the density plots of the three different products. The correlation of LST_{MW} against LST_{MD} is much lower, with 0.64 and 0.26 for both regions, showing a low relation in the Catchment. LST_{E5} compares better to LST_{MD} with a correlation of 0.70 in the Catchment and 0.65 in the Delta, however this is still significantly lower than the comparison with LST_{MW}. The absolute ranges in the anomalies as detected by the three products are very similar.

The slightly lower correlation of LST_{MW} against LST_{E5} in the Delta is mostly caused by the period 2010 and 2011, when the LST_{E5} anomaly (between -1 and 1 °C) is smaller than that of LST_{MW} (between -3 and -1 °C). This break away is clearly visible in the density plot of Fig. 4F on the lower left side. Below-average temperatures are recorded for a prolonged period between 2006 and 2014 in both regions. For the Delta, the highest temperature anomalies are recorded in 2019 and 1998. In the Catchment, this is seen in 2015 and 2019.

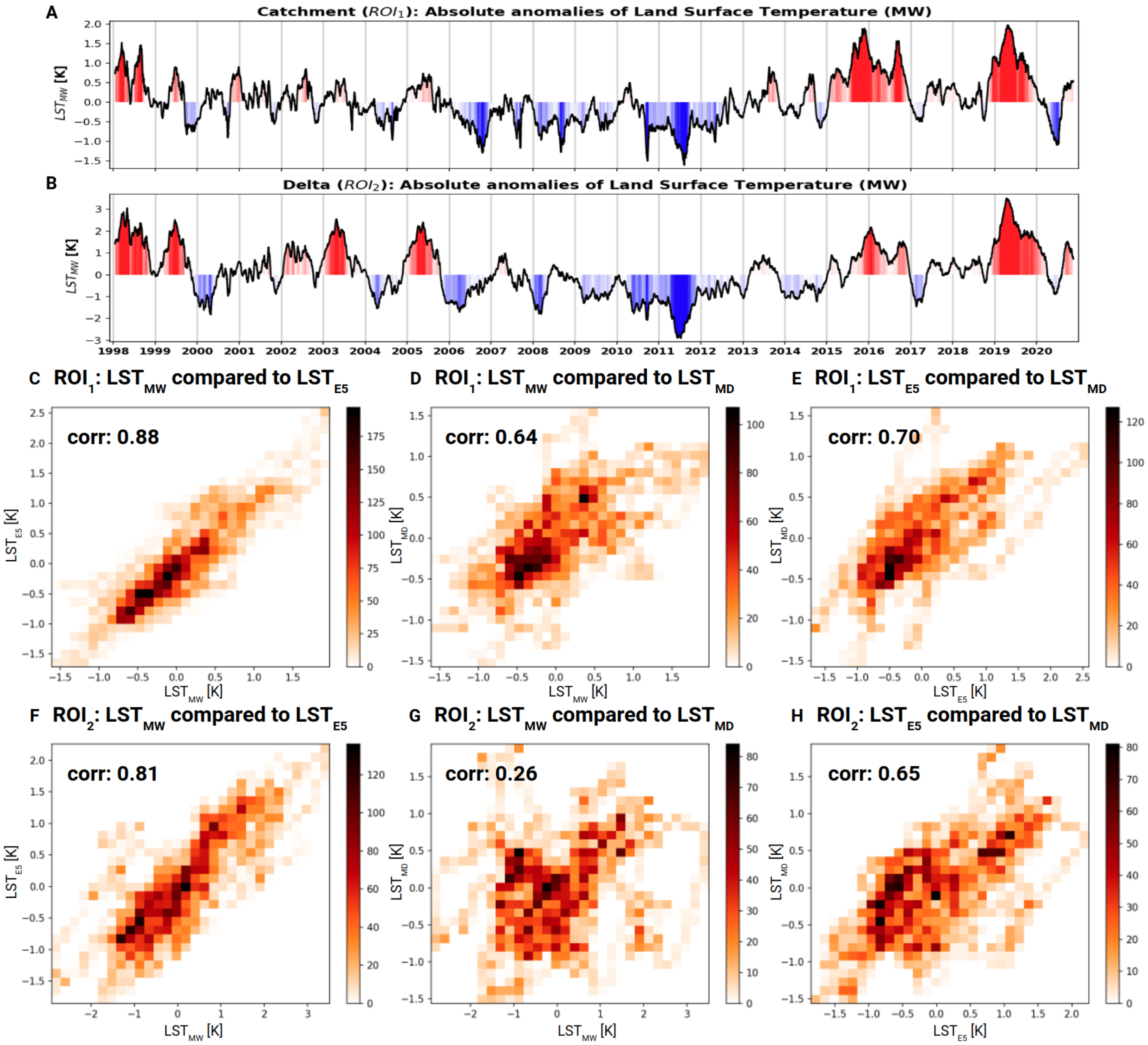

Figure 4: LST$_{MW}$ time series over the Okavango Catchment and the Okavango Delta (A,B), with the intensity of the colouring based on the z-score of the positive (red) and negative (blue) anomalies. For the density plots; LST$_{MW}$ compared to LST$_{E5}$ (C,F), LST$_{MW}$ compared to LST$_{MD}$ (D,G), LST$_{E5}$ compared to LST$_{MD}$ (E,H). A daily time step is used from the moving average data set for the density plots.

4.4 River and precipitation contribution to soil moisture anomalies in the Okavango Delta

Figure 5A, 5B and 5C show the anomalies of the ORD, ODIA$_{MD}$ and PR$_{E5}$ over the Delta, which have visibly different signals. The ORD shows a strong multi-year signal with especially high values recorded from 2009 to 2012. Outside of that period, with the exception of 2004, values generally lay below the 2003 to 2020 climatology. The OIAD$_{MD}$ shows a signal that is relatively similar to that of the ORD, however smoother, with less variability and lagging behind. The PR$_{E5}$ over the Delta shows mostly values around 0 mm during this 2009 to 2012 period, and otherwise varies more dynamically from year to year with values above and below the climatology.

Although SSM$_{MW}$ and SSM$_{E5}$ anomalies have an overall correlation of 0.69 in the Delta, Figure 2F shows many occasions where the SSM$_{MW}$ had negative or positive anomalies, while the SSM$_{E5}$ did not diverge from the climatology. To better assess what causes this opposite signal, the climatology (using ±15 days moving average) of different parameters are provided in Figure 6, including their 10% and 90% percentiles. Here one can see the difference in the dynamics between SSM$_{MW}$ (Fig. 6A) and SSM$_{E5}$ (Fig. 6B). The SSM$_{E5}$ shows a clear relation to the PR datasets (Fig. 6G/H), while the SSM$_{MW}$ still picks up a moisture signal between April and September. When looking at the ORD and OIAD$_{MD}$, these are the moisture-related signals that still show strong variability in this time of the year, indicating that the SSM$_{MW}$ could also contain information from other sources than PR. On a side note, Figure 6 shows that besides matching well with long term anomalies, LST$_{MW}$ and VOD$_{MW}$ also have a strong matching intraseasonal signal with LST$_{E5}$ and LAI$_{MD}$, respectively.

Table 2 presents the results of a multiple linear regression to determine the drivers of the observed/modelled SSM anomaly signal in the Delta, using ODIA$_{MD}$, ORD and PR as inputs. The Z-score anomalies are used to improve the comparability between the different datasets and their weight. The results show that the weighting for SSM$_{MW}$ consists of a balance between the PR in the Delta and the ODIA$_{MD}$, with an overall slightly higher weight for the ODIA$_{MD}$, and leading to a maximum correlation of 0.84 when using PR$_{E5}$ over PR$_{IM}$. This leads to a RMSE of about 0.44 for the Z-score. The SSM$_{E5}$ anomalies are clearly driven by the PR$_{E5}$ anomalies, reaching a correlation of 0.87. The correlation strongly decreases to 0.64 when the PR$_{E5}$ is replaced with PR$_{IM}$, which reflects back in the RMSE of the Z-score anomalies, which increases from about 0.37 to 0.57.

Table 2: Results of the multiple linear regression for estimating the relationships between the Z-score anomalies of SSM, PR, ORD, and ODIA$_{MD}$ over ROI$_2$.

Prediction	Input 1	Input 2	Correlation	RMSE	Weight input 1	Weight input 2
SSM$_{MW}$	PR$_{E5}$	ORD	0.78	0.49	0.53	0.58
	PR$_{IM}$	ORD	0.70\	0.50	0.49	0.52
	PR$_{E5}$	ODIA$_{MD}$	0.84	0.43	0.44	0.67
	PR$_{IM}$	ODIA$_{MD}$	0.81	0.44	0.40	0.67
SSM$_{E5}$	PR$_{E5}$	ORD	0.87	0.37	0.88	0.17
	PR$_{IM}$	ORD	0.64	0.57	0.74	0.16
	PR$_{E5}$	ODIA$_{MD}$	0.87	0.38	0.88	0.16
	PR$_{IM}$	ODIA$_{MD}$	0.65	0.56	0.71	0.19

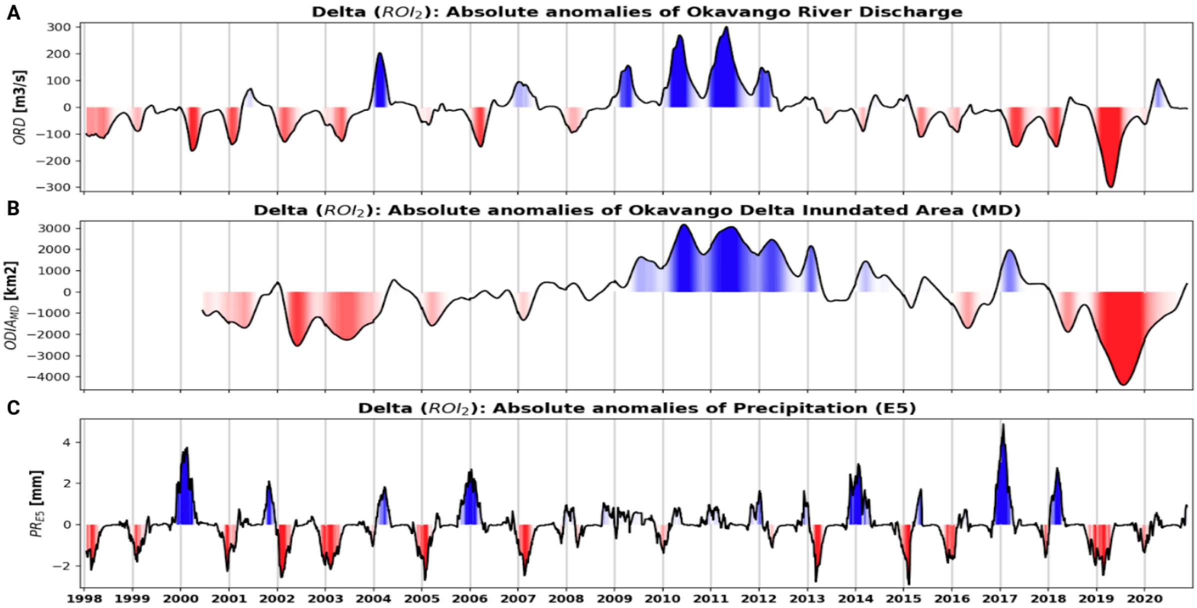

Figure 5: ORD, ODIA$_{MD}$ and PR$_{E5}$ time series over the Okavango Delta (A,B,C), with the intensity of the colouring based on the z-score of the positive (blue) and negative (red) anomalies.

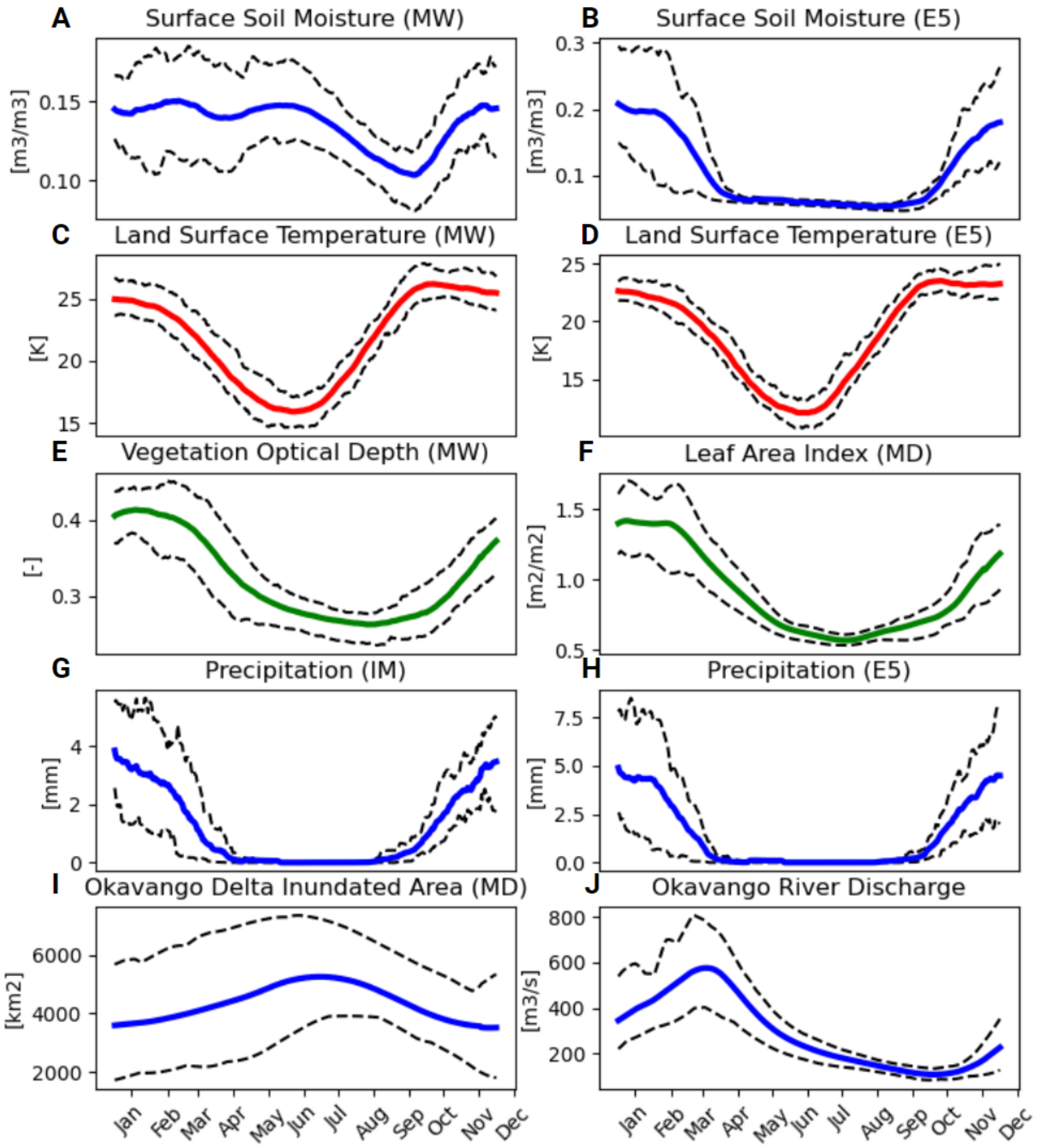

Figure 6: ROI$_2$ mean climatology (colored thick line) and both 10% and 90% percentiles (black dashed lines) for SSM$_{MW}$ (A), SSM$_{E5}$ (B), LST$_{MW}$ (C), LST$_{E5}$ (D), VOD$_{MW}$ (E), LAI$_{MD}$ (F), PR$_{IM}$ (G), PR$_{E5}$ (H), ODIA$_{MD}$ (I) and ORD (J). Data using a ±15 days moving average was plotted to distinguish between intraseasonal signals.

5 Discussion

Over both the Delta and the Catchment, a remarkably strong relationship between the LAI$_{MD}$ and VOD$_{MW}$ was observed, even though fundamentally they measure two different things. The relationship is slightly weaker over the Catchment, where you see more of a buffer effect in the VOD$_{MW}$ dataset as compared to the LAI$_{MD}$. This could be caused by a buildup of woody biomass, as this would theoretically be better detected with the VOD$_{MW}$ than with the LAI$_{MD}$. The period of sustained high VOD$_{MW}$ in the catchment during the 2008 to 2012 period aligns well with the PR_{E5}, which recorded 5 years of above-average rainfall over the Catchment. The ORD shows this increase above the climatology starting only the year afterwards (from 2009 to 2012), showing the lagged response of the system after a prolonged dryer period.

The VOD_{MW} signal in the Delta is more complex: the peaks in VOD_{MW} do not coincide with prolonged time spans of high water availability, but seem to peak during shorter periods of increased water availability during overall conditions with medium to low $ODIA_{MD}$. This can be explained by what the VOD represents: in this case, it is related to biomass that is above the surface. During prolonged periods of high water, a larger extent of these regions are flooded. Therefore, within the 0.25° pixel, data that is not corrected for dynamic water bodies, the vegetation covered by these flooded areas might not be properly measured by the VOD_{MW} signal. As it is also known that VOD_{MW} values can be underestimated during flooded conditions (Bousquet et al., 2021). Note that the negative SSM_{MW} and ORD anomalies in 2019 have not led to the same intensity of vegetation decline, while in 2019 the $ODIA_{MD}$ was at a record low in the last 20 years. With the very strong relationship over the Delta between the anomalies of both VOD_{MW} and LAI_{MD} - two independent satellite-observed datasets - these observations very likely reflect the conditions on the ground. These results show that future use of even longer VOD_{MW} records can help monitor complex regions like the Okavango Catchment and Delta. For example, following the progress on VODCA -which aims to build a data record similar to the ESA CCI SSM for VOD_{MW} -future releases will also include the latest calibrated datasets as used here.

Three different sources of LST were tested over the Okavango Catchment and Delta. The highest correlation can be found between the LST_{E5} and LST_{MW}, which most likely best represent the actual ground conditions. Although LST_{MD} performs less well, the better correlation of LST_{MD} against LST_{E5} than LST_{MW} might indicate that the overall best performing dataset is the LST_{E5}. However, in many cases an observation-based long term dataset (e.g. the LST_{MW}) is still preferred. For example, in 2010 and 2011 the LST_{MW} has the lowest temperature anomalies on record in the Delta, going to -3 K, while the LST_{E5} remains more neutral. This is most likely caused by the lack of lateral water influx modelling from the ORD and following $ODIA_{MD}$ in ERA5-Land (Muñoz-Sabater et al., 2021), as shown in Section 4.4. The lack of moisture input into the model can lead to an underestimation of the latent heat flux and overestimation of the sensible heat flux, leading to an unrealistically high LST_{E5}.

In the Delta, 2015, 2016, and 2019 have been warm compared to the years before. The LST_{MW} and LST_{E5} both show that these are not unique occurences, as similar high values have been detected on multiple occasions before 2006. These seem to occur during periods of lower $ODIA_{MD}$, which shows dry anomalies of varying strength in these years. The catchment does see its highest and more prolonged peaks only in the last years, i.e. 2015 and 2019. These high peaks coincide with the strongest negative anomalies found for both SSM_{MW} and SSM_{E5}, linking the high temperature and reduced moisture availability.

The precipitation-driven SSM in the Catchment aligns closely with SSM_{MW} and SSM_{E5} datasets. Especially in the period after 2010, the signal in the anomalies is very similar. Before 2010, it appears that the SSM_{MW} shows slightly stronger dynamics than SSM_{E5}. In the Delta a mismatch is clearly seen between SSM_{E5} and SSM_{MW}, especially with regard to the duration of the dry and wet peaks, but also in their intensity. With the knowledge that about 50%-75% of the water flux into the Delta comes from the ORD, and about 25%-50% from the PR, an analysis using Z-score anomalies was conducted to determine the driving signals behind the SSM anomalies, using the ORD, $ODIA_{MD}$ and PR as inputs. For SSM_{E5}, an almost one-to-one relationship was found with the PR, with little to no effects from the ORD or $ODIA_{MD}$. The SSM_{MW} anomalies on the other hand, are almost equally driven by PR and $ODIA_{MD}$, which is much closer to the actual balance between the ORD and PR water fluxes for the Delta as expected from literature.

The almost one-to-one relationship between the SSM_{E5} and PR_{E5}, and lack of signal related to the ORD due to the missing lateral water influx modelling, or alternatively dynamic open water bodies using the $ODIA_{MD}$, in ERA5-Land indicates that in a complex region like the Okavango Delta important forcings are missing. This for example could also cause the difference in LST_{MW} and LST_{E5} in 2010 and 2011 (not shown), as the model cannot correctly convert the incoming radiation into sensible and latent heat fluxes when the moisture conditions are inaccurate, leading to a false increase of LST. On the other hand, while the SSM_{MW} signal provides users with a better representation of total moisture conditions within the catchment, it can also not be interpreted as a pure SSM signal here, as it includes moisture information driven by the $ODIA_{MD}$. In a dynamic environment as the Okavango Delta, users should therefore clearly define what they require of such datasets to avoid unwanted side effects.

6 Conclusion

The anomalies of three different parameters, i.e. SSM_{MW}, LST_{MW} and VOD_{MW}, were evaluated against other satellite-observed data sets and data from the ERA5-Land climate reanalysis. Although SSM_{MW} and SSM_{E5} correlate moderately well, structural differences were detected over the Okavango Delta, where SSM_{MW} contains a clear multi-year signal that is not in the SSM_{E5}. To determine the cause of this mismatch, an analysis was conducted to determine the impact of three sources of water into the Okavango Delta, i.e. the ORD, $ODIA_{MD}$ and the PR, on the SSM signal. The SSM_{MW} signal appears to be driven about equally by the $ODIA_{MD}$ and the PR, while SSM_{E5} is almost fully driven by the PR_{E5}. This indicates that ERA5-Land does not properly include the lateral influx of the Okavango River, and therefore the use of SSM_{MW} is preferred in this region.

For the VOD_{MW}, a direct comparison against LAI_{MD} was made. Although the two parameters measure two different physical characteristics of the vegetation, their anomalies show a similar response, which were reflected back in their strong correlations (0.74 and 0.88) . Over the Catchment, a stronger multi-year signal was detected in the VOD_{MW}, which could be related to the build up of biomass, to which VOD_{Mw} is theoretically more sensitive. For the Delta, both datasets are impacted by the increase in open water during long wet periods that can suppress the observed vegetation. This strong similarity as observed between the two datasets, indicate that it is very likely they are both representative for the in situ conditions.

LST_{MW} was shown to be of good quality and correlated well with LST_{E5} (>0.8). LST_{MD} still managed to reach a significant correlation with LST_{E5}, but not with LST_{MW}, indicating that in general LST_{E5} could be of highest quality of the three when looking at the temporal signal. However, at the record-low values in LST_{MW} over the Delta in 2010-11, corresponding to the peak years of the ORD and $ODIA_{MD}$, it seems that LST_{E5} cannot properly model the sensible and latent heat fluxes because it is missing the lateral water component. This can have a large impact for detecting extremes, which are especially important in the current changing climate.

The findings of this research show the importance of not only relying on climate reanalysis, but also the need for further development and maintenance of observational datasets like the ones derived from passive microwave observations. For example within the ESA CCI Soil Moisture datasets, but also the development of new CDRs on VOD_{MW} like VODCA. Their ability to properly detect anomalies and extremes is very valuable in climate research, and can especially help to improve our insight in complex regions where the current climate reanalysis datasets reach their limitations. With microwave data being available from 1978 onwards, the data can be used for long-term climate studies, near-real-time applications, e.g. monitoring complex natural systems like the Okavango Delta, and to constrain climate reanalysis through data assimilation techniques to overcome known model weaknesses.

7 Author Contributions

RS is the main author of this manuscript, and led the conceptualization, data curation, formal analysis, validation, visualisation, and writing of the original draft. MV provided support for the conceptualization of the study and contributed to the writing and the visualisation in Sect. 2, on the research area. CA supported this study by reviewing the manuscript and reforming the conceptualization to better put the research in perspective of the scientific community. WD contributed by extensively reviewing the manuscript. PW provided support in the understanding of the Okavango region, data provision for $ODIA_{MD}$, and reviewing of the manuscript. RJ was active in the conceptualization of the study and writing of the Introduction.

8 Competing interests

The authors declare that they have no conflict of interest.

9 Acknowledgments

This study and the authors were supported by ESA’s Climate Change Initiative for Soil Moisture (Contract No. 4000104814/11/I-NB and 4000112226/14/I-NB).

10 References

Al-Yaari, A., Wigneron, J.P., Dorigo, W., Colliander, A., Pellarin, T., Hahn, S., Mialon, A., Richaume, P., Fernandez-Moran, R., Fan, L. and Kerr, Y.H., 2019. Assessment and inter-comparison of recently developed/reprocessed microwave satellite soil moisture products using ISMN ground-based measurements. Remote sensing of environment, 224, pp.289-303.

Albergel, C., Dorigo, W., Reichle, R.H., Balsamo, G., De Rosnay, P., Muñoz-Sabater, J., Isaksen, L., De Jeu, R. and Wagner, W., 2013. Skill and global trend analysis of soil moisture from reanalyses and microwave remote sensing. Journal of Hydrometeorology, 14(4), pp.1259-1277.

Ashton, P. J., & Manley, R. E., 1999, November. Potential hydrological implications of water abstraction from the Okavango River in Namibia. In Proceedings of the Ninth South African Hydrological Symposium.

Ashton, P. 2003., The search for an equitable basis for water sharing in the Okavango River basin. International Waters in Southern Africa, pp.164-188.

Ashton, P. and Neal, M., 2003. An overview of key strategic issues in the Okavango basin. Transboundary rivers, sovereignty and development: Hydropolitical drivers in the Okavango River basin, pp.31-63.

Ashworth, M., 2002. Hydrology. Maun Groundwater Development Programme (MGDP) Phase 2. Gaborone: Water Resources Consultants.

Beck, H.E., Pan, M., Miralles, D.G., Reichle, R.H., Dorigo, W.A., Hahn, S., Sheffield, J., Karthikeyan, L., Balsamo, G., Parinussa, R.M. and van Dijk, A.I., 2021. Evaluation of 18 satellite-and model-based soil moisture products using in situ measurements from 826 sensors. Hydrology and Earth System Sciences, 25(1), pp.17-40.

Berg, W., Bilanow, S., Chen, R., Datta, S., Draper, D., Ebrahimi, H., Farrar, S., Jones, W.L., Kroodsma, R., McKague, D. and Payne, V., 2016. Intercalibration of the GPM microwave radiometer constellation. Journal of Atmospheric and Oceanic Technology, 33(12), pp.2639-2654.

Bojinski, S., Verstraete, M., Peterson, T.C., Richter, C., Simmons, A. and Zemp, M., 2014. The concept of essential climate variables in support of climate research, applications, and policy. Bulletin of the American Meteorological Society, 95(9), pp.1431-1443.

Chen, J.M.; Black, T.A. Defining leaf area index for non-flat leaves. Plant Cell Environ. 1992, 15, 421–429.

Cook, B. I., Slinski, K., Peters-Lidard, C., McNally, A., Arsenault, K., & Hazra, A. (2021). The Efficacy of Seasonal Terrestrial Water Storage Forecasts for Predicting Vegetation Activity over Africa. Journal of Hydrometeorology, 22(11), 3121-3137.

Dorigo, W.A., Gruber, A., De Jeu, R.A.M., Wagner, W., Stacke, T., Loew, A., Albergel, C., Brocca, L., Chung, D., Parinussa, R.M. and Kidd, R., 2015. Evaluation of the ESA CCI soil moisture product using ground-based observations. Remote Sensing of Environment, 162, pp.380-395.

Dorigo, W., Wagner, W., Albergel, C., Albrecht, F., Balsamo, G., Brocca, L., Chung, D., Ertl, M., Forkel, M., Gruber, A. and Haas, E., 2017. ESA CCI Soil Moisture for improved Earth system understanding: State-of-the art and future directions. Remote Sensing of Environment, 203, pp.185-215.

Gruber, A., Scanlon, T., van der Schalie, R., Wagner, W. and Dorigo, W., 2019. Evolution of the ESA CCI Soil Moisture climate data records and their underlying merging methodology. Earth System Science Data, 11(2), pp.717-739.

Gumbricht, T., Wolski, P., Frost, P. and McCarthy, T.S., 2004. Forecasting the spatial extent of the annual flood in the Okavango Delta, Botswana. Journal of Hydrology, 290(3-4), pp.178-191.

Hersbach, H., Bell, B., Berrisford, P., Hirahara, S., Horányi, A., Muñoz-Sabater, J., Nicolas, J., Peubey, C., Radu, R., Schepers, D. and Simmons, A., 2020. The ERA5 global reanalysis. Quarterly Journal of the Royal Meteorological Society, 146(730), pp.1999-2049.

Hirschi, M., Nicolai-Shaw, N., Preimesberger, W., Scanlon, T., Dorigo, W. and Kidd, R., 2021. Product Validation and Intercomparison Report (PVIR), Supporting Product version v06.1, Deliverable ID: D4.1 Version 2.

Hollmann, R., Merchant, C.J., Saunders, R., Downy, C., Buchwitz, M., Cazenave, A., Chuvieco, E., Defourny, P., de Leeuw, G., Forsberg, R. and Holzer-Popp, T., 2013. The ESA climate change initiative: Satellite data records for essential climate variables. Bulletin of the American Meteorological Society, 94(10), pp.1541-1552.

Holmes, T.R.H., Crow, W.T., Hain, C., Anderson, M.C. and Kustas, W.P., 2015. Diurnal temperature cycle as observed by thermal infrared and microwave radiometers. Remote Sensing of Environment, 158, pp.110-125.

Holmes, T.R.H., De Jeu, R.A.M., Owe, M. and Dolman, A.J., 2009. Land surface temperature from Ka band (37 GHz) passive microwave observations. Journal of Geophysical Research: Atmospheres, 114(D4).

Huffman, G.J., Bolvin, D.T., Braithwaite, D., Hsu, K., Joyce, R., Xie, P. and Yoo, S.H., 2015. NASA global precipitation measurement (GPM) integrated multi-satellite retrievals for GPM (IMERG). Algorithm Theoretical Basis Document (ATBD) Version, 4, p.26.

Imaoka, K., Maeda, T., Kachi, M., Kasahara, M., Ito, N. and Nakagawa, K., 2012, November. Status of AMSR2 instrument on GCOM-W1. In Earth Observing Missions and Sensors: Development, Implementation, and Characterization II (Vol. 8528, p. 852815). International Society for Optics and Photonics.

Jackson, T.J. and Schmugge, T.J., 1991. Vegetation effects on the microwave emission of soils. Remote Sensing of Environment, 36(3), pp.203-212.

Kawanishi, T., Sezai, T., Ito, Y., Imaoka, K., Takeshima, T., Ishido, Y., Shibata, A., Miura, M., Inahata, H. and Spencer, R.W., 2003. The Advanced Microwave Scanning Radiometer for the Earth Observing System (AMSR-E), NASDA's contribution to the EOS for global energy and water cycle studies. IEEE Transactions on Geoscience and Remote Sensing, 41(2), pp.184-194.

Kgathi, D.L., Kniveton, D., Ringrose, S., Turton, A.R., Vanderpost, C.H.M., Lundqvist, J. and Seely, M., 2006. The Okavango; a river supporting its people, environment and economic development. Journal of Hydrology, 331(1-2), pp.3-17.

Kummerow, C., Barnes, W., Kozu, T., Shiue, J. and Simpson, J., 1998. The tropical rainfall measuring mission (TRMM) sensor package. Journal of atmospheric and oceanic technology, 15(3), pp.809-817.

Liu, Y.Y., Dorigo, W.A., Parinussa, R.M., de Jeu, R.A., Wagner, W., McCabe, M.F., Evans, J.P. and Van Dijk, A.I.J.M., 2012. Trend-preserving blending of passive and active microwave soil moisture retrievals. Remote Sensing of Environment, 123, pp.280-297.

Liu, Y.Y., Van Dijk, A.I., De Jeu, R.A., Canadell, J.G., McCabe, M.F., Evans, J.P. and Wang, G., 2015. Recent reversal in loss of global terrestrial biomass. Nature Climate Change, 5(5), pp.470-474.

Liu, Y.Y., van Dijk, A.I., McCabe, M.F., Evans, J.P. and de Jeu, R.A., 2013. Global vegetation biomass change (1988–2008) and attribution to environmental and human drivers. Global Ecology and Biogeography, 22(6), pp.692-705.

Loew, A., Stacke, T., Dorigo, W., Jeu, R.D. and Hagemann, S., 2013. Potential and limitations of multidecadal satellite soil moisture observations for selected climate model evaluation studies. Hydrology and Earth System Sciences, 17(9), pp.3523-3542.

McCarthy, T. S., Bloem, A., & Larkin, P. A. 1998. Observations on the hydrology and geohydrology of the Okavango Delta. South African Journal of Geology, 101(2), pp.101-117.

McCarthy, T.S., Cooper, G.R.J., Tyson, P.D. & Ellery, W. 2000. Seasonal flooding in the Okavango Delta, Botswana-recent history and future prospects. South African Journal of Science, 96(1), pp.25-33.

McCarthy, J. M., Gumbricht, T., McCarthy, T., Frost, P., Wessels, K., & Seidel, F. 2003. Flooding patterns of the Okavango wetland in Botswana between 1972 and 2000. Ambio: A journal of the human environment, 32(7), pp.453-457.

Meesters, A.G., De Jeu, R.A. and Owe, M., 2005. Analytical derivation of the vegetation optical depth from the microwave polarization difference index. IEEE Geoscience and Remote Sensing Letters, 2(2), pp.121-123.

MGDP, 1997. Maun Groundwater Project Phase 1: Exploration and Resource Assessment – Executive Summary. Gaborone: Department of Mineral, Energy and Water Affairs.

Mo, T., Choudhury, B.J., Schmugge, T.J., Wang, J.R. and Jackson, T.J., 1982. A model for microwave emission from vegetation-covered fields. Journal of Geophysical Research: Oceans, 87(C13), pp.11229-11237.

Moesinger, L., Dorigo, W., de Jeu, R., van der Schalie, R., Scanlon, T., Teubner, I. and Forkel, M., 2020. The global long-term microwave vegetation optical depth climate archive (VODCA). Earth System Science Data, 12(1), pp.177-196.

Muñoz Sabater, J., (2019): ERA5-Land hourly data from 1981 to present. Copernicus Climate Change Service (C3S) Climate Data Store (CDS). (Accessed on 1-Aug-2021), 10.24381/cds.e2161bac

Muñoz-Sabater, J., Dutra, E., Agustí-Panareda, A., Albergel, C., Arduini, G., Balsamo, G., Boussetta, S., Choulga, M., Harrigan, S., Hersbach, H., Martens, B., Miralles, D. G., Piles, M., Rodríguez-Fernández, N. J., Zsoter, E., Buontempo, C., and Thépaut, J.-N.: ERA5-Land: a state-of-the-art global reanalysis dataset for land applications, Earth Syst. Sci. Data, 13, 4349–4383, https://doi.org/10.5194/essd-13-4349-2021, 2021.

Muzungaire, L., Mebelo, W., Shuuluka, D. and Omoregie, E., 2012. Preliminary investigation of biomagnifications of trace metals in the Okavango River, North-eastern Namibia. Research Journal of Agricultural and Environmental Management Vol, 1(2), pp.034-042.

Okavango Research Institute, 2021. http://okavangodata.ub.bw/ori/monitoring/water/# (visited on 20-Aug-2021).

Owe, M., de Jeu, R. and Holmes, T., 2008. Multisensor historical climatology of satellite-derived global land surface moisture. Journal of Geophysical Research: Earth Surface, 113(F1).

Preimesberger, W., Scanlon, T., Su, C.H., Gruber, A. and Dorigo, W., 2020. Homogenization of Structural Breaks in the Global ESA CCI Soil Moisture Multisatellite Climate Data Record. IEEE Transactions on Geoscience and Remote Sensing, 59(4), pp.2845-2862.

Republic of Botswana, 2013. Okavango Delta World Heritage Nomination Dossier, Nomination dossier to UNESCO for inscription into the World Heritage List. (https://whc.unesco.org/uploads/nominations/1432.pdf visited at 19-Aug-2021)

Ringrose, S., Matheson, W. and Boyle, T., 1988. Differentiation of ecological zones in the Okavango Delta, Botswana by classification and contextural analyses of Landsat MSS data. Photogrammetric Engineering and Remote Sensing, 54(5), pp.601-608.

Rodríguez-Fernández, N.J., Mialon, A., Mermoz, S., Bouvet, A., Richaume, P., Al Bitar, A., Al-Yaari, A., Brandt, M., Kaminski, T., Le Toan, T. and Kerr, Y.H., 2018. An evaluation of SMOS L-band vegetation optical depth (L-VOD) data sets: high sensitivity of L-VOD to above-ground biomass in Africa. Biogeosciences, 15(14), pp.4627-4645.

Scanlon, T., Pasik, A., Dorigo, W., De Jeu, R.A.M., Hahn, S., Van der Schalie, R., Wagner, W., Kidd, R., Gruber, A., Moesinger, L. and Preimesberger, W., 2021. ESA Climate Change Initiative Plus - Soil Moisture, Algorithm Theoretical Baseline Document (ATBD), Supporting Product Version 06.1, D2.1 Version 2.

Schwank, M., Kontu, A., Mialon, A., Naderpour, R., Houtz, D., Lemmetyinen, J., Rautiainen, K., Li, Q., Richaume, P., Kerr, Y. and Mätzler, C., 2021. Temperature effects on L-band vegetation optical depth of a boreal forest. Remote Sensing of Environment, 263, p.112542.

Teubner, I.E., Forkel, M., Camps-Valls, G., Jung, M., Miralles, D.G., Tramontana, G., Van der Schalie, R., Vreugdenhil, M., Mösinger, L. and Dorigo, W.A., 2019. A carbon sink-driven approach to estimate gross primary production from microwave satellite observations. Remote Sensing of Environment, 229, pp.100-113.

Van der Schalie, R., De Jeu, R.A., Kerr, Y.H., Wigneron, J.P., Rodríguez-Fernández, N.J., Al-Yaari, A., Parinussa, R.M., Mecklenburg, S. and Drusch, M., 2017. The merging of radiative transfer based surface soil moisture data from SMOS and AMSR-E. Remote Sensing of Environment, 189, pp.180-193.

Van der Schalie, R., Scanlon, T.M., Preimesberger W., Pasik, A.J., Van der Vliet, M., Mösinger, L., Rodríguez-Fernández, N.J., Madelon, R., Hahn, S., Hirschi, M., Kidd, R., De Jeu, R.A.M., and Dorigo, W.A., 2021: Soil moisture [in “State of the Climate in 2020”]. Bull. Amer. Meteor., 102 (8), S67, https://doi.org/10.1175/BAMS-D-21-0098.1.

Van der Schalie, R., Van der Vliet, M., Rodríguez-Fernández, N., Dorigo, W.A., Scanlon, T., Preimesberger, W., Madelon, R. and de Jeu, R.A., 2021. L-band soil moisture retrievals using microwave based temperature and filtering. Towards model-independent climate data records. Remote Sensing, 13(13), p.2480.

Van Marle, M.J., Field, R.D., van der Werf, G.R., de Wagt, I.A.E., Houghton, R.A., Rizzo, L.V., Artaxo, P. and Tsigaridis, K., 2017. Fire and deforestation dynamics in Amazonia (1973–2014). Global biogeochemical cycles, 31(1), pp.24-38.

Wan, Z., 2014. New refinements and validation of the collection-6 MODIS land-surface temperature/emissivity product. Remote sensing of Environment, 140, pp.36-45.

Wolski, P. and Murray-Hudson, M., 2008. Alternative futures' of the Okavango Delta simulated by a suite of global climate and hydro-ecological models. Water SA, 34(5), pp.605-610.

Wolski, P., Murray-Hudson, M., Thito, K., & Cassidy, L. (2017). Keeping it simple: Monitoring flood extent in large data-poor wetlands using MODIS SWIR data. International journal of applied earth observation and geoinformation, 57, 224-234.

Wolski, P., Savenije, H. H., Murray-Hudson, M., & Gumbricht, T. (2006). Modelling of the flooding in the Okavango Delta, Botswana, using a hybrid reservoir-GIS model. Journal of Hydrology, 331(1-2), 58-72.

Wolski, P., Stone, D., Tadross, M., Wehner, M. and Hewitson, B., 2014. Attribution of floods in the Okavango basin, Southern Africa. Journal of Hydrology, 511, pp.350-358.

Wolski, P., Todd, M.C., Murray-Hudson, M.A. and Tadross, M., 2012. Multi-decadal oscillations in the hydro-climate of the Okavango River system during the past and under a changing climate. Journal of Hydrology, 475, pp.294-305

Yang, W., Tan, B., Huang, D., Rautiainen, M., Shabanov, N.V., Wang, Y., Privette, J.L., Huemmrich, K.F., Fensholt, R., Sandholt, I. and Weiss, M., 2006. MODIS leaf area index products: From validation to algorithm improvement. IEEE Transactions on Geoscience and Remote Sensing, 44(7), pp.1885-1898.